Comparison of Measured Neutron Yield Versus Pressure Curves for FMPF-3, NX2 and NX3 Plasma Focus Machines Against Computed Results Using the Lee Model Code

10 authors, including:

Sor Heoh Saw
Nilai University, Negeri Sembilan, Malaysia
98 PUBLICATIONS   905 CITATIONS

R.S. Rawat
National Institute of Education (NIE), Singa…
286 PUBLICATIONS   2,759 CITATIONS

Rishi Verma
Bhabha Atomic Research Centre
57 PUBLICATIONS   230 CITATIONS

Raju Khanal
Tribhuvan University
19 PUBLICATIONS   52 CITATIONS

Comparison of Measured Neutron Yield Versus Pressure Curves for FMPF-3, NX2 and NX3 Plasma Focus Machines Against Computed Results Using the Lee Model Code

S. H. Saw · P. Lee · R. S. Rawat · R. Verma ·
D. Subedi · R. Khanal · P. Gautam ·
R. Shrestha · A. Singh · S. Lee

Abstract A range of plasma focus machines from the 200 J FMPF3 through the 2 kJ NX2 to the 20 kJ NX3 are operated at the National Institute of Education in Singapore. The neutron yield Y_n versus pressure P curves for these machines have been measured and published. We use the Lee code to compute these Y_n versus P curve for each machine after fitting a computed current waveform to a current waveform measured from each machine. Comparison of computed with measured Y_n versus P curves show good agreement of peak Y_n for the NX2 and NX3 whilst the measured peak Y_n of FMPF3 is larger than the computed by a factor of 3. The computed curve is generally broader whilst the NX3 computed curve also shows a shift to higher pressures than the measured curve. The results are critically discussed.

Keywords Plasma focus · Plasma focus modeling · Plasma focus neutrons · Lee model code · Neutron yield versus pressure

S. H. Saw · A. Singh · S. Lee (✉)
INTI International University, 71800 Nilai, Malaysia
e-mail: leesing111@yahoo.com; leesing@optusnet.com.au

S. H. Saw · S. Lee
Institute for Plasma Focus Studies, 32 Oakpark Drive,
Chadstone, VIC 3148, Australia

P. Lee · R. S. Rawat
National Institute of Education, Nanyang Technological
University, Singapore 637616, Singapore

R. Verma
Bhaba Atomic Research Centre, Autonagar,
Visakhapatnam 530012, India

D. Subedi · R. Shrestha
Department of Natural Science, Kathmandu University,
Dhulikhel, Nepal

R. Khanal · P. Gautam
Central Department of Physics, Tribhuvan University, Kirtipur,
Kathmandu, Nepal

S. Lee
Universty of Malaya, Kuala Lumpur, Malaysia

Introduction

Of the copious multi-radiations from the plasma focus, arguably the most important is the neutron emission, with its tantalizing promise of nuclear fusion energy applications. The building up of a database of nuclear fusion neutrons from plasma focus is therefore important. One fundamental question such a database could help to answer is whether modelling of focus fusion neutrons should be based on the mechanism of thermonuclear fusion or beam-plasma target fusion. One of the earliest modelling efforts was by Potter [1] who used a two-fluid MHD model to comprehensively discuss with great insight many aspects of flow dynamics within the plasma focus pinch. His conclusion was that using a thermonuclear mechanism he could explain the measured D–D neutron yield from the specific plasma focus he was modelling. Although the insights Potter extracted regarding the temperature and density profiles and the two-dimensional flows within the pinch column remain unmatched to this day, his conclusion of a predominantly thermonuclear fusion mechanism within focus pinch was likely influenced by estimates of flow velocities of too high a magnitude. More recently Moreno et al. [2] and Gonzalez et al. [3] used modelling codes based on thermonuclear fusion mechanism which adjusted axial and radial mass sweeping factors in

individual machines until computed Y_n agrees with measured Y_n. Moreover their computation of shock speeds was based on a 1983 version of a code by Lee [4] which did not include the crucial feature of 'communication delay' between the shock front and driving magnetic piston in the radial plasma slug [5–8], thus overestimating the shock speed by factor 2, shock temperature by factor 4 and D–D fusion cross-section by factor exceeding 1,000 [8]. The Lee code [6, 7] has since 1995 included this 'communication delay' with results (in terms of dynamics and radiation yields) which are consistent with experiments [8].

A 2009 paper by Gonzalez et al. [9] used Von Karman approximations of radial velocity and density profiles with four parameters namely axial shape parameter, radial shape parameter, velocity profile exponent and density profile exponent *which are fitted to the measured Y_n versus P curve* of the seven machines they examined using a thermonuclear mechanism. There is no mention in the paper of testing any other results of the modelling against measured experiment; nor of any predictive capabilities of the model in respect of any property or any other machine even for neutron yield.

On the other hand the Lee Model code [6, 7] uses four parameters, two axial mass and current factors and two radial mass and current factors to fit a computed current trace to the measured current trace of any plasma focus. The argument is that the current waveform carries in its wave shape information on all the processes occurring within the discharge, including the dynamics, energetics, thermodynamics and radiation. Once the computed current waveform is fitted to the measured, the configured plasma focus is equivalent energy-wise, charge-wise, momentum-wise and mass-wise to the actual plasma focus; all these processes having been taken care of by the adjustment of the four parameters and the code which models the dynamics, electrodynamics, thermodynamics and radiation interactively. Once the computed current waveform is fitted to the measured, it has been found that the dynamics, thermodynamics, soft X-rays, fusion neutrons (in D and D–T) and ion and plasma properties in various gases are consistent with observed values.

From accumulated experimental data on neutron pulse characteristics, spectra and spatial anisotropy of emission and yields, mechanisms such as moving boiler, beam-target, gyrating particles, Quasi-Maxwellian hot plasmoids [10–15] are proposed. In the light of the data it may be concluded that the predominant mechanism is non-thermonuclear. For example Moo et al. [13] used target techniques to conclude that more than 85 % of the D–D neutrons are due to beam-plasma target mechanisms. We had incorporated a beam-plasma target mechanism similar to the one described by Gribkov et al. [12] into the Lee code [6, 7]. The code also includes a thermonuclear fusion mechanism. The Lee code has successfully been used to obtain the scaling laws of plasma focus neutron yields [16–22] and soft X-rays [21–24] and scaling trends of ions as functions of PF energy, total current and pinch current. [25–27]. It has been used to compute neutron yields for comparison with measured values [8, 28] and also to explain the deterioration of Y_n as a function of E_0 [18].

In this paper we use the Lee code on a series of three machines operating in Singapore to compute the respective Y_n versus P curve and compare with the corresponding measured Y_n versus P curve. The machines are the 0.2 kJ FMPF3 [29], the 2.5 kJ NX2 [30, 31] and the 20 kJ NX3 (operating at 10 kJ) [32, 33] from which the data for this paper has been collected and combined with new numerical experiments using the Lee code to generate new results.

Procedure

In each case we configure the code to the specific machine. We input the capacitor bank parameters, the focus tube parameters and the operational parameters. We have a measured current waveform which has an approximate calibration factor. We start with trial values of the four model parameters and sequentially adjust these parameters starting with f_m, f_c, then f_{mr} and f_{cr}, fitting firstly the current waveform for the axial phase and then the current dip which corresponds with the radial phase. In practice we try as far as possible to keep f_c and f_{cr} at value of 0.7 to simplify the procedure, consistent with experimental observations [34, 35, 37]. We use the measured amplitude of the current waveform as a guide, but where the measured amplitude differs from the computed we use the computed amplitude as the correct value. The rationale for this is that the code uses charge-consistent equations and given a known starting quantity of charge in the capacitor, once we have fitted the shape of the computed current waveform to the shape of the measured current waveform, the area under the current profile is given by the charge that has flowed out of the capacitor up to that given time. Since the code is charge-consistent its computed amplitude of current is a correct value. We thus use the code to calibrate the amplitude of the current waveform once the waveform shape is corrected fitted. We use the 5-phase code which fits the dip up to the end of the radial phase. We do not attempt to fit the current trace beyond the end of the computed radial phase. In the fitting procedure we allow the computed current waveform to be shifted as a whole relative to the measured current waveform to account for the imperfect switching action of the switch, in this case pseudo-spark switches. We also apply a current factor to the measured current waveform so as to calibrate the measured current amplitude to that of the computed. When

the fit is completed we have the four model parameters for the specific plasma focus. The code is then run at different pressures giving the Y_n at each P. The computed Y_n versus P curve is then compared with the measured Y_n versus P curve.

Results

FMPF-3

FMPF-3 is a 200 J plasma focus designed for repetitive operation as a portable neutron source. It uses a stainless steel anode.

The plasma focus configuration is recorded as follows:

Bank parameters: $L_0 = 34$ nH, $C_0 = 2.4$ μF, $r_0 = 11$ mΩ.

Tube parameters: $b = 1.5$ cm, $a = 0.6$ cm, $z_0 = 1.7$ cm.

Operation parameters: $V_0 = 13$ kV, $P_0 = 3.38$ Torr, MW = 4, A = 1, At/Mol = 2.

Tapered anode: start of taper is at taper start = 1 cm and tapered end radius = 0.37 cm.

A measured current waveform is available at 13 kV 4.5 mbar. The computed current waveform is fitted to the measured current waveform. The fit is reasonable for the important regions of the topping profile, the top profile and the current dip. No attempt is made to fit beyond the end of radial phase; and any divergence or agreement of the computed with measured beyond the end of the radial phase is not considered significant.

There is considerable difference in the first 0.12 μs (computed trace) due to the non-ideal switching characteristics of PSS as opposed to perfect switching assumed in the code (Fig. 1).
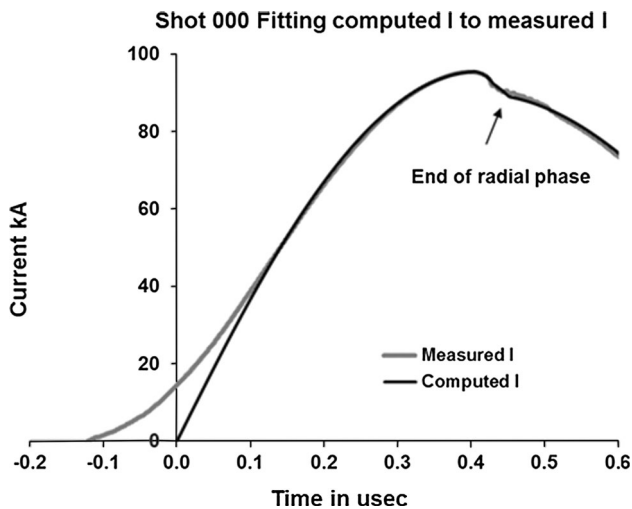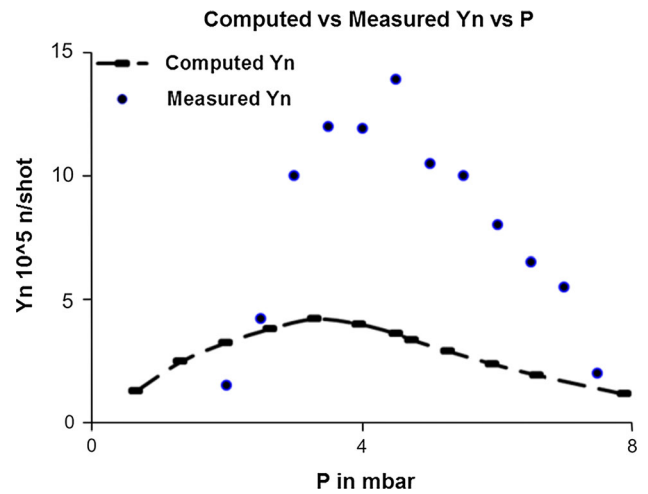

Fig. 1 Fitting of FMPF3 at 3.4 Torr deuterium

Fig. 2 Computed Y_n versus P compared with measured Y_n versus P for FMPF-3

It is found that the fit of the shape of the current waveform is very good up to the end of the pinch phase. From this fit, the model parameters are found to be: $f_m = 0.15$, $f_c = 0.7$, $f_{mr} = 0.55$, $f_{cr} = 0.7$. We note that the current calibrated to the computed charge has an error due to the first part of current waveform which could not be fitted. This error is less than 3 %.

Using these parameters for the series at different pressures, the computed Y_n are obtained for each pressure. The computed Y_n versus P curve is plotted and compared with the measured Y_n versus P curve as shown in Fig. 2.

From the comparison we find that the computed curve agrees with the measured curve in terms of general shape with the computed peak value of Y_n occurring at nearly 4 mbar compared to the measured peak values occurring at about 4 mbar. The peak computed value of Y_n is 1/3 that of the measured value. The measured peak has a double peak appearance whereas the computed is single-peaked. The computed values of Y_n is typically within a factor less than 3 of the measured value in the pressure range of 2–8 mbar. The measured curve peaks more sharply than the computed curve.

NX2

The NX2 is a repetitive plasma focus designed originally as a high performance neon soft X-ray SXR source for microlithography. The original design incorporates water-cooling to run the plasma focus at 16 Hz (2 kJ storage energy) 400 kA peak current with 20 J neon SXR per shot. It has been re-designed to operate efficiently as a neutron source as well.

The configuration of NX2 for this series of experiments is as follows:

Bank parameters: $L_0 = 20$ nH, $C_0 = 28$ μF, $r_0 = 2.7$ mΩ.

Fitting computed to measured I waveforms
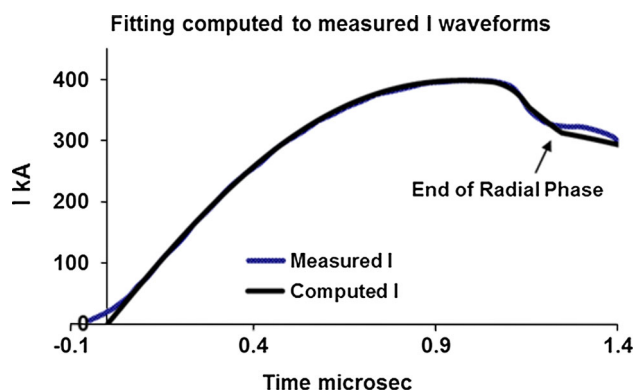
Fig. 3 Fitting of NX2 at 15 Torr deuterium

Fitting Computed to Measured I Waveforms

Fig. 5 Fitting of current waveform for NX3 at 14 kV 4.6 Torr deuterium, using anode configuration A20Z140. This current waveform is typical of NX3 for operation between 2 and 8 Torr deuterium [32]. For this configuration the anode has an effective length of 12.6 cm

Tube parameters: b = 3.8 cm, a = 1.55 cm, z_0 = 4.5 cm.

Operation parameters: V_0 = 14.5 kV, P_0 = 15 Torr, MW = 4, A = 1, At/Mol = 2.

Tapered anode: taperstart = 1 cm and end radius = 1.15 cm.

A measured current trace is available at 14.5 kV 20 mbar = 15 Torr.

The computed current waveform is fitted to the measured waveform in Fig. 3. The fit is good up to the end of the radial pinch phase. No attempt has been made to fit beyond end of radial phase. Similar to the case of the fitting of FMPF3, there is a similar divergence in the first 0.1 μs. The divergence appears relatively minor in this case, because the time scale is three times bigger as well as the scale of current which is also three times larger. The computation of current amplitude is more accurate in this case. The current fitting reveals that the model parameters are: f_m = 0.11, f_c = 0.7, f_{mr} = 0.38, f_{cr} = 0.7.

We ran numerical experiments using these model parameters over a range of pressures. We obtain the computed Y_n versus P curve which is shown in Fig. 4 and compared with the measured Y_n versus P curve.
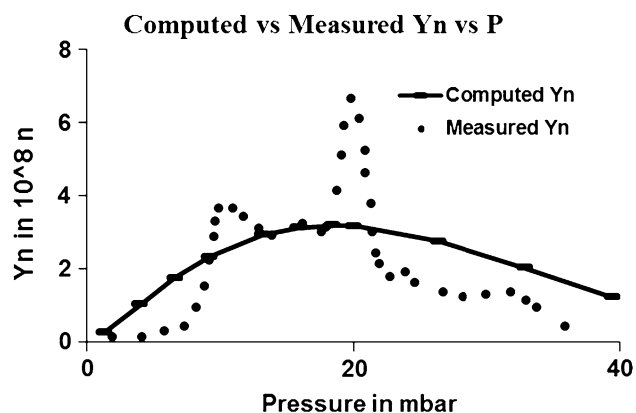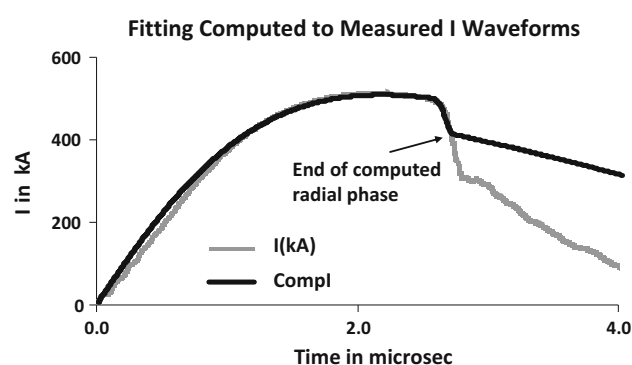
Computed vs Measured Yn vs P

Fig. 4 Computed Y_n versus P compared to measured Y_n versus P for NX2

From the comparison we find that the computed curve agrees with the measured curve in terms of general shape with the computed peak value of Y_n occurring at 17 mbar compared to the measured peak values occurring at 19 mbar. The peak computed value of Y_n is 1/2 that of the measured value. The measured peak has a double peak appearance whereas the computed is single-peaked. The computed values of Y_n is typically within a factor less than 2 of the measured value in the pressure range of 9–35 mbar. The measured curve peaks more sharply than the computed curve.

NX3

The NX3 uses a low inductance 20 kV capacitor bank with 20 kJ at maximum charging voltage. We have a current waveform at 14 kV [32].

The relevant configuration is as shown:

Bank parameters: L_0 = 30 nH, C_0 = 100 μF, r_0 = 2.3 mΩ.

Tube parameters: b = 5.6 cm, a = 2 cm, z_0 = 12.6 cm.

Operation parameters: V_0 = 14 kV, P_0 = 4.6 Torr, MW = 4, A = 1, At/Mol = 2.

The computed current waveform is fitted to the measured waveform, shown in Fig. 5.

The fit is good up to the end of the radial pinch phase. No attempt is made to fit beyond the end of the computed radial phase. The current fitting reveals that the model parameters are: f_m = 0.255, f_c = 0.7, f_{mr} = 0.0.26, f_{cr} = 0.7.

We ran numerical experiments using these model parameters over a range of pressures. We obtained the computed Y_n versus P curve which is shown in Fig. 6 and compared with the measured Y_n versus P curve for anosed configuration A20Z140 [33].

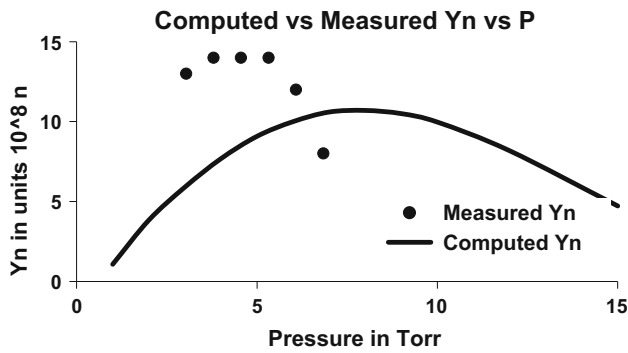From the comparison we find that the computed curve agrees with the measured curve in terms of general shape

Fig. 6 Computed Y_n versus P compared to measured Y_n versus P for NX3, A20Z140 anode configuration

with the computed peak value of Y_n occurring at 8 Torr compared to the measured peak values occurring at 5–6 Torr. The peak computed value of Y_n is close to that of the measured value. The measured peak has a single flattened peak appearance similar to the computed which is also single-peaked. The computed values of Y_n is typically within a factor less than 2 of the measured value in the measured pressure range of 3–7 Torr. The measured curve peaks more sharply than the computed curve.

Conclusion and Discussion

In this paper we have analysed the computed Y_n versus P results by comparing with the measured Y_n versus P for 3 machines operating at Singapore NTU/NIE Plasma Radiation Sources Lab over a range of energies of 200 J to 12 kJ. The comparison shows that the computed Y_n versus P has a much gentler slope on each side of the maximum compared with the measured Y_n versus P curve. The computed curve peaks at a pressure which is higher than the measured optimum pressure by a factor up to two. The computed optimum value of Y_n is in all three cases less than the measured by a factor of 1.5–3. Over the range of pressures the computed value of neutron yield at any pressure is comparable to the measured neutron yield better than a factor of 3. These and earlier [8] results show that once the code is fitted to the measured current waveform, the code is able to estimate neutron yields to better than a factor of 3. The computed also give the correct trends for the Y_n versus P with a computed optimum typically lower than the measured and occurring at a lower pressure than the measured optimum. The indications are that: (1) The code averages the physical profiles (of temperatures and densities) and the averaging has the effect of smoothening out the profiles, giving much gentler variation than observed experimentally. (2) A closer study of the results shows that the code continues to estimate high values of Y_n

at pressures considerably beyond time-matched pressures whereas experimentally Y_n is found to drop more sharply after peak value. This indicates that there are finer mechanisms working to limit Y_n at pressures beyond time-matched and that these mechanisms are either not modelled within the code or not completely taken care of in the procedures of the numerical experiments.

The computed neutron yield is predominantly from the following mechanism [6, 7].

$$Y_{b-t} \sim \mathbf{n_i} I_{pinch}^2 z_p^2 \left(\ln \left(b/r_p \right) \right) \sigma / V_{max}^{0.5}$$

Here I_{pinch} is the current flowing through the pinch at start of the slow compression phase; r_p and z_p are the pinch dimensions at end of that phase. One key factor affecting the neutron yield is I_{pinch}. As the operational pressure is increased past the time-matched point the current sheet speed drops due to the dependence of the speed factor S on the pressure [34, 35]. The magnetic Reynold's number which is proportional to speed to the power of 4 [36] drops much more rapidly. When this number is no longer much greater than unity the electromagnetic drive deteriorates. Experimentally this decreased efficiency of coupling may act to reduce the neutron yield. The code does include this effect through the 4 model parameters (mass and current factors). For example a lower current factor will reduce the value of I_{pinch}. Al-Hawat et al. [37] have shown the variation of the axial mass parameter with pressure. However because we typically have only one measured current waveform we have kept these model parameters constant throughout the pressure range using the factors obtained from that waveform near time-matched conditions. These model parameters that we use reflect good drive efficiency; and since we continue to use these model parameters at higher pressures we attribute higher drive efficiency to our computed yield at higher pressures than actually exists. Hence the computed yield versus pressure curve may drop more slowly at higher pressures than that of the measured yield versus pressure curve.

In this respect it would be better to obtain the model parameters for each pressure. This would require a measured current waveform and fitting at each pressure that the neutron yield is measured.

References

1. D.E. Potter, Phys. Fluids **14**, 1911 (1971)
2. C. Moreno, H. Bruzzone, J. Martínez, A. Clausse, IEEE Trans. Plasma Sci. **28**, 1735 (2000)

3. J.H. Gonzalez, A. Clausse, H. Bruzzone, P.C. Florido, IEEE Trans. Plasma Sci. **32**, 1383 (2004)
4. Lee S, in Proc. 1983 College on Plasma Physics, ICTP (Trieste, Italy) Radiations in Plasmas vol 2 ed B McNamara (Singapore: World Scientific, 1984) pp 978–87
5. D.E. Potter, Nucl. Fusion **18**, 813–823 (1978)
6. S. Lee, Radiative Dense Plasma Focus Computation Package: RADPF (2000–2014). http://www.plasmafocus.net; http://www.intimal.edu.my/school/fas/UFLF/ (archival websites)
7. S. Lee, J. Fusion Energ. **33**, 319–335 (2014). doi:10.1007/s10894-014-9683-8
8. S. Lee, S.H. Saw, L. Soto, S.V. Springham, S.P. Moo, Plasma Phys. Control. Fusion **51**, 075006 (2009)
9. J.H. González, F.R. Brollo, A. Clausse, IEEE Trans. Plasma Sci. **37**, 11 (2009). doi:10.1109/TPS.2009.2030578
10. A. Bernard et al., J. Mosc. Phys. Soc. **8**, 93–170 (1998)
11. M. Krishnan, IEEE Trans. Plasma Sci. **40**(12), 3189–3221 (2012)
12. V.A. Gribkov et al., J. Phys. D Appl. Phys. **40**, 3592 (2007)
13. S.P. Moo, C.K. Chakrabarty, S. Lee, IEEE Trans. Plasma Sci. **19**, 515 (1991)
14. S.V. Springham, S. Lee, M.S. Rafique, Plasma Phys. Control. Fusion **42**, 1023 (2000)
15. E Lerner arXiv:physics/0401126 (2004)
16. S. Lee, S.H. Saw, J. Fusion Energ. **27**, 292–295 (2008)
17. S. Lee, Plasma Phys. Control. Fusion **50**, 10500 (2008)
18. S. Lee, Appl. Phys. Lett. **95**, 151503 (2009)
19. S.H. Saw, S. Lee, Energ. Power Eng. **2**(1), 65–72 (2010)
20. S. Lee, S.H. Saw, Special edition on ''Fusion Energy''. Energies **3**, 711–737 (2010). doi:10.3390/en3040711
21. S.H. Saw, S. Lee, Int. J. Energ. Res. **35**, 81–85 (2011). doi:10.1002/er.1758
22. S. Lee, S.H. Saw, Int. J. Energ. Res. **36**(15), 1366–1374 (2012)
23. S. Lee, S.H. Saw, P. Lee, R.S. Rawat, Plasma Phys. Control. Fusion **51**, 105013 (2009)
24. M. Akel, S. Lee, S.H. Saw, IEEE Trans. Plasma Sci. **40**, 3290–3297 (2012)
25. S. Lee, S.H. Saw, Phys. Plasmas **19**, 12703 (2012). doi:10.1063/1.4766744
26. S. Lee, S.H. Saw, Phys. Plasmas **20**, 062702 (2013). doi:10.1063/1.4811650
27. M. Akel et al., J. Fusion Energ. (2014). doi:10.1007/s10894-013-9660-7
28. S.H. Saw et al., J. Fusion Energ. (2014). doi:10.1007/s10894-014-9731-4
29. Rishi Verma, R.S. Rawat, P. Lee, S.V. Springham, T.L. Tan, J. Fusion Energ. **32**, 2–10 (2013). doi:10.1007/s10894-012-9517-5
30. J.M. Koh et al., Plasma Sour. Sci. Technol. **14**, 12–18 (2005). doi:10.1088/0963-252/14/1/002
31. S. Lee, P. Lee, G. Zhang, X. Feng, V.A. Gribkov, M. Liu, A. Serban, T. Wong, IEEE Trans. Plasma Sci. **26**, 1119 (1998)
32. M. Rasyid et al to be published
33. R. Verma et al., Plasma Sci. IEEE Trans. Plasma Sci. **40**(12), 3280–3289 (2012). doi:10.1109/TPS.2012.2220569
34. S. Lee, A. Serban, IEEE Trans. Plasma Sci. **24**, 1101–1105 (1996)
35. S. Lee, S.H. Saw, H. Hegazy, J. Ali, V. Damideh, N. Fatis, H. Kariri, A. Khubrani, A. Mahasi, J. Fusion Energ. **33**(3), 235–241 (2014). doi:10.1007/s10894-013-9658-1
36. S. Lee, S.H. Saw, P.C.K. Lee, R.S. Rawat, K. Devi, J. Fusion Energ. **32**, 50–55 (2013). doi:10.1007/s10894-012-9521-9
37. S. Al-Hawat et al., J. Fusion Energ. **31**, 13–20 (2012). doi:10.1007/s10894-011-9414-3-3